Carboxyl Tail Prevents Yeast K^+ Channel Closure: Proposal of an Integrated Model of TOK1 Gating

Stephen H. Loukin and Yoshiro Saimi
Laboratory of Molecular Biology, University of Wisconsin, Madison, Wisconsin 53706 USA

ABSTRACT *TOK1* encodes the channel responsible for the prominent outward K^+ current of the yeast plasma membrane. It can dwell in several impermeable states, including a rapidly transiting, K^+-electromotive-force-dependent "R" (*r*ectifying) state, a voltage-independent "IB" (*i*nter*b*urst) state, and a set of $[K^+]_{ext}$ and voltage-dependent "C" (*c*losed) states. Whereas evidence suggests that the C states result from the constriction of an inner gate at the cytosolic end of the pore, R is most likely an intrinsic gating property of the K^+ filter. Here, we present evidence that Tok1's carboxyl-tail domain also plays an intimate role in channel gating by dynamically preventing inner-gate closures. We present an integrated model of TOK1 gating in which the filter gate, inner gate, and carboxyl tail interact to produce the various phenomenological states. Both wild-type and tailless behaviors can be replicated using Monte Carlo computer simulations based on this model.

INTRODUCTION

TOK1 (*YKC1*, *DUK1*, "York") encodes the outwardly rectifying K^+ channel in the plasma membrane of the budding yeast *Saccharomyces cerevisiae* (Reid et al., 1996; Zhou et al., 1995). It is predicted to possess a "dual P region" structure containing a K_v-like six-transmembrane (TM) core followed by an additional P region and flanked by two additional TMs (see Fig. 2) (Ketchum et al., 1995). Similarly structured dual-P-region channels have been identified in the genomes of prokaryotes (Derst and Karschin, 1998) while dual-P-region channels possessing only four transmembrane domains have been characterized in a wide variety of eukaryotic cells (Czempinski et al., 1997; Duprat et al., 1997; Maingret et al., 2000; Zilberberg et al., 2000).

Ensemble episodic recordings reveal at least two distinct types of impermeable states of TOK1 (Loukin et al., 1997; Fig. 1): a near-instantaneously transiting, K^+-electrochemical-force ($\Delta\mu_{K^+}$)-dependent "R" state, which rapidly blocks inward current flow under any K^+ conditions, and C, a set of related, slowly transiting states in which TOK1 dwells in response to negative membrane potential and high external K^+ ($[K^+]_{ext}$). TOK1 dwells in C and R at potentials mildly negative to the K^+-equilibrium potential (E_K), but the C states dominate at more negative potentials and in higher $[K^+]_{ext}$ (Lesage et al., 1996; Vergani et al., 1997). Viewed at the single channel level, TOK1 rapidly flickers at a frequency of ~1 kHz (Gustin et al., 1986).

Evidence suggests that TOK1 has at least two gates. The R state is most easily interpreted as an intrinsic gating property of the filter region itself (Loukin and Saimi, 1999). Genetic evidence suggests that the C state closures result from a constriction of the inner mouth of the channel pore, akin to deactivation-type gating in other cation channels (Loukin et al., 1997). Mutations in the "post-pore" or "PP" region, the cytoplasmic end of the membrane-spanning domain following either of the P regions, curtails distribution into C but has little effect on R-state behavior. This same region appears to gate other cation channels. Access to the PP region of *Shaker* by bulky modifying reagents has been shown to be deactivated-state-dependent (Liu et al., 1997) and modification of the region affects gating parameters of both rod and olfactory cyclic nucleotide-gated channels (Gordon and Zagotta, 1995a, b).

It is becoming increasingly evident that the cytoplasmic domains of cation channels often play key roles in their gating. The carboxyl tail of the high-conductance K^+ channel, Slo1, dramatically affects its Ca^{2+}-dependent gating, most likely by stabilizing closed states in the absence of

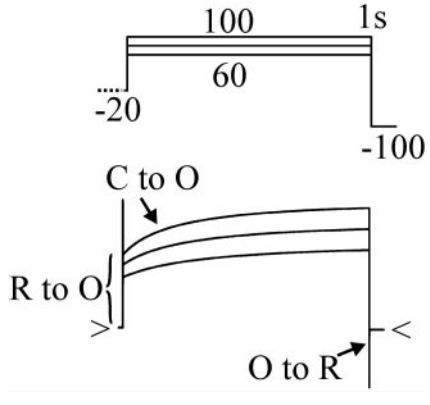

FIGURE 1 The R and C states of TOK1. Upon depolarization from mildly negative holding potentials, TOK1 activates from two distinct closed states. Activation from the R state ("R to O") is marked by a seemingly instantaneous surge in current from 0 (horizontal carat). Activation from C ("C to O") is marked by time dependent increase in conductance. Upon repolarization, current "instantaneously" returns to 0 reflecting a rapid return to the R state ("O to R"). Currents were recorded from a whole *TOK1* expressing oocyte bathed in 100 mM KCl, 1 mM $MgCl_2$, 1 mM $CaCl_2$, and 5 mM HEPES, pH 7.5.

Submitted July 9, 2001, and accepted for publication October 5, 2001.

Address reprint requests to S. H. Loukin, Laboratory of Molecular Biology, University of Wisconsin, 1525 Linden Dr., Madison, WI 53706. Tel.: 608-262-7976; Fax: 608-262-4570; E-mail: shloukin@facstaff.wisc.edu.

0006-3495/02/02/781/12 $2.00

Ca^{2+} (Schreiber et al., 1999). The carboxyl tail of cyclic nucleotide-gated (CNG) channels interacts with the amino terminus to stabilize the open state of the channel (Varnum and Zagotta, 1997). Evidence suggests that phosphorylation of the carboxyl tail of Kv2.1 affects its own gating (Murakoshi et al., 1997). The amino cytoplasmic "T1" domains of the Kv1 channel have been shown in elegant experiments to interact with each other to stabilize the closed channel conformation (Cushman et al., 2000; Minor et al., 2000). Gating functions of the carboxyl tail of four-TM, dual-P-region channels have also been demonstrated; the tail of the KCNKØ (ORK1) leak channel is required for maintenance of the long-lived closed state (Zilberberg et al., 2000) and that of the mechano-gated, heat-activated channel TREK1 is required for lipid, acid (Maingret et al., 1999; Patel et al., 1999), and high temperature-dependent (Maingret et al., 2000) activation.

In an attempt to further define the region(s) involved in internal-pore gating, intragenic suppressors of a TOK1 PP mutant were isolated. The comprehensive results of this study, which is still in progress, will be reported in the future. Common among the suppressors were mutations that delete a majority of the carboxyl tail. We found that deletion of the carboxyl tail has dramatic effects on TOK1 gating as reported here. Analysis of the effects of tail deletion has led us to develop an integrated model of Tok1 gating in which the filter's gate, the internal gate, and the carboxyl tail interact to produce the multiple observed phenomenological states of TOK1.

MATERIALS AND METHODS

Isolation of TOK1 T322I revertants

The pGALYKC-301 plasmid contains a galactose-inducible T332I "PP"-mutant allele of *TOK1* that blocks proliferation when expressed in yeast (Loukin et al., 1997). pGALYKC1-301 was mutagenized by propagating the plasmid in the XL1-Red bacterial strain (Stratagene, La Jolla, CA) containing mutations in the primary DNA repair pathways. The extent of mutagenesis was quantitated as a 2% loss-of-*URA3* function monitored by transformation a bacterial *pyrf* strain (Bach et al., 1979). Mutated pGALYKC1-301 plasmids were transformed into the *TOK1* deletion strain αku8 (Zhou et al., 1995). After initial colony formation under permissive conditions ($uracil^-$, glucose), colonies were replica plated onto *TOK1-T322I*-restrictive conditions ($uracil^-$, galactose) additionally containing 100 mM LiCl. The LiCl was used because it was found that *TOK1* deletion causes a sensitivity to Li^+ (Saimi, unpublished observation), and loss-of-TOK1-function would be the most common cause of T322I reversion because $TOK1^-$ strains are perfectly viable. Plasmids were isolated from colonies that proliferated on the galactose, Li^+ plates and double-strand sequenced by standard techniques. Common among the T322I revertants were those that contained mutations which deleted a large portion of the predicted carboxyl-terminus.

Expression of TOK1

One of the revertants, Q456*, was randomly chosen for further analysis from the carboxyl-tail deletants. The double T322I/Q456* mutation was subcloned from the yeast-expression plasmid to the oocyte-expression plasmid pGH19 as described in Loukin et al., 1997. A Q456* allele (without T322I) was generated by reverting the AA322 to Thr using standard PCR-mutagenesis techniques. In vitro RNA synthesis and oocyte isolation, injection, and maintenance were as described previously (Loukin et al., 1997). For wild-type TOK1 analysis, ~10 ng of RNA was injected per oocyte. For most of the Q546* analysis, ~100 ng RNA was injected for ensemble recordings. For single channel analysis, ~100-fold less RNA was injected.

Electrophysiological recordings

Both macro-patch and single channel patch recordings were performed as described elsewhere (Loukin et al., 1997). In all cases pipette (external) solutions contained 140 mM monovalent chloride salts (either K^+ or *N*-methyl D-glucamine (NMG^+)), 1 mM $MgCl_2$, 1 mM $CaCl_2$, and 5 mM HEPES, pH 7.5, and the bath (internal) solutions all contained 140 mM KCl, 4 mM $MgCl_2$, 1 mM $CaCl_2$, 5 mM HEPES, and 5 mM EGTA, pH 7.5. All recordings were carried out at 21–22°C, which is important to monitor due to the high degree of temperature sensitivity of C-state transition rates.

Computer simulations

Monte Carlo simulations of channel activity were conducted using a Visual Basic program written by S. Loukin. The program allows up to a 10×10 array of states, which can be connected to up to four individual neighboring states. Transitions between two states can either be defined by forward and reverse time constants or by voltage-dependent parameters, V_{50}, and the degree of voltage dependence, δ. Using the simplifying assumption that voltage-dependent transition occurs infinitely faster than the transitions defined by rate constants, states related by voltage-dependent transitions were treated as a single state. Voltage-dependent distribution between states A and B was calculated by $A/B = 10^{(V\text{-}V50)/(\delta*58)}$, where V_{50} and V (the test potential) are given in millivolts and a δ value of 1 being equivalent to a unit positive charge crossing the entire voltage field.

At the start of each sweep, an array containing the running probability of being in any state was determined based on defined transition rates and defined voltage-dependent distribution at the assigned holding potential using the formula stated above. The starting holding state was then assigned by where a random roll landed within this running-probability array. Also assigned at the beginning of the simulation was a "chance of exit" array containing the probability of leaving each state (P_1) within an assigned tick-length (t, usually set to 1 ms):

$$P_1 = 1 - \exp(-(k_1 + k_2 \cdots + k_i) \cdot t)$$

where k_1 through k_i are the exit rate constants from the state. An "exit-state" array containing the running relative probabilities of which state was exited to based on individual rates and voltage dependence was calculated for each state was also calculated at the start. These arrays were initialized at the start to avoid redundant calculations within the simulation.

Single sweeps were calculated as follows. For each tick of the simulation, if a random role between 0 and 1 was larger than the probability value in the "chance of exit" array for the current state, then the tick was advanced and the roll repeated until it was smaller than the probability value. At that point, the state that was exited into was assigned by where a random roll fell within the running "exit-state" probability array. Multichannel simulations were performed by the summing of single channel simulations.

The R-state is modeled as not being an equilibrium process, and therefore could not be realistically simulated using these algorithms. Its behavior was approximated by making the transition between R and O voltage-dependent, with a V_{50} of 0 mV and a δ of 1, and forcing a return from O to R within the next 1-ms tick.

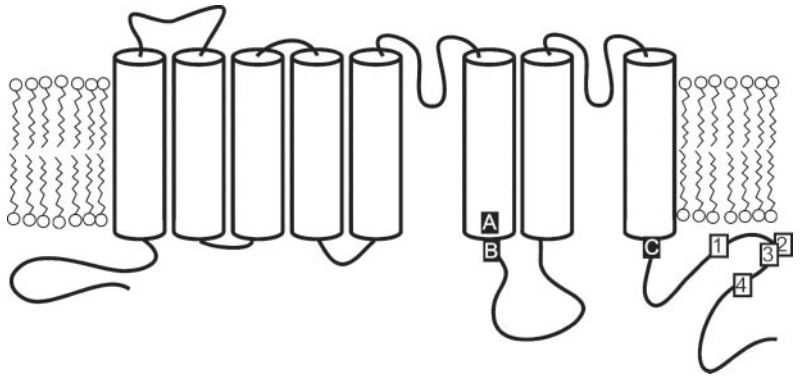

FIGURE 2 PP and tail deletion mutants of TOK1. Hydropholicity and homology predict that TOK1 is an eight-transmembrane protein with repeated P-regions following the fifth and seventh transmembrane domains. Location of growth blocking post-pore "PP" mutants are T322I (*A*), S330F (*B*), and V456I (*C*). Isolated loss-of-tail mutants that rescued the T322I allele are Q546* (1), S577-point deletion (2), G578-point deletion (3), and Q586* (4).

RESULTS

Deletion of the carboxyl tail rescues a C-state mutant of TOK1

Upon depolarization from mildly negative holding potentials, TOK1 activates from two kinetically distinct nonconducting states, "R" and "C". Activation from R is marked by a rapid ($\sim 10^4$ s^{-1}; Loukin and Saimi, 1999) surge in conductance, which appears instantaneous in standard traces (Fig. 1, "R to O"). "Instantaneous" deactivation to the R state can likewise be observed upon repolarization (Fig. 1, "O to R"). Activation from the C states occurs much more slowly and often requires multiple activation rates to describe adequately (Fig. 1, "C to O"). An outstanding feature of TOK1 is that its dwell in R is dependent on the entire transmembrane $\Delta\mu_{K^+}$ (ibid.), allowing outward but not inward conductance. Dwell in C, however, is dependent on external $[K^+]$ ($[K^+]_{ext}$) and negative membrane potential (V_m), but *not* internal $[K^+]$ (Loukin and Saimi, 1999). In 140 mM symmetrical K^+, channels are equally distributed between the R and C states at -20 mV, but almost exclusively in C at -100 mV.

Point mutations in the post-pore "PP" region, the cytoplasmic end of the membrane-spanning domain following either of the P loops (Fig. 2), specifically interfere with the C states, not R (Loukin et al., 1997). One PP mutant, T322I, was used as a basis for an ongoing intragenic suppressor analysis to further define regions involved in C-state gating. Conditional expression of T322I blocks yeast proliferation. Intragenic, second-site mutations were isolated that overcame T322I's growth-blocking effect without destroying overall channel function. Common among these suppressors were mutations that result in deletion of a substantial proportion of the carboxyl tail (Fig. 2).

Consistent with its ability to alleviate growth inhibition, tail deletion restored the C state to the T322I mutant. Wild-type channels activate almost exclusively from the C state when depolarized from -100 mV in 140 mM $[K^+]_{ext}$, activating increasingly from R when depolarized from more positive holds (Fig. 3 *A*, "wild-type"). PP mutation shifts this voltage dependence of C distribution leftward, such that even from a -100 mV hold, the majority of the channels activate from R (Fig. 3 *A*, "PP"). Tail deletion caused by suppressing Q546* mutation more than restored the ability of the T322I mutant to dwell in C (Fig. 3 *A*, "PP/tailless")

Tail deletion causes a large positive shift in the voltage dependence of C dwell

The effect of tail deletion alone on channel activity was examined. Initially it appeared that these channels were nonfunctional. Little current was observed in the standard voltage ramps from -90 to $+90$ mV. Outward currents were observed, though, when oocytes were injected with higher levels of tailless cRNA and at more positive depolarizations than required to observe wild-type currents (Fig. 3 *B*). These currents were not due to activation of endogenous oocyte currents resulting from high-level expression of heterologous membrane proteins. Injection of similar levels of RNA from several nonconducting alleles did not result in such outward conductance (S. Loukin, unpublished observations). Additionally, the observed tailless current is of similar unitary conductance to wild-type TOK1 (Fig. 5), displays a similar unique instantaneous closure upon repolarization (Fig. 4 *D*), has the same single channel "flickery" behavior, and has very different kinetics and rectification from the induced endogenous oocyte currents described elsewhere (Shimbo et al., 1995; Tzounopoulos et al., 1995).

The lack of conductance through the tailless channel at mildly positive potentials is due to the channel dwelling in C. When stepped from a hold of 80 mV, which is 60 mV positive to a potential at which wild-type channels are near-maximally partitioned out of C, all of the tailless channels activated with C-type slow kinetics (Fig. 3 *B*). Wild-type channels have an apparent V_{50} of C distribution of -12 ± 15 mV ($n = 4$) in symmetrical 140 mM K^+ (Fig.

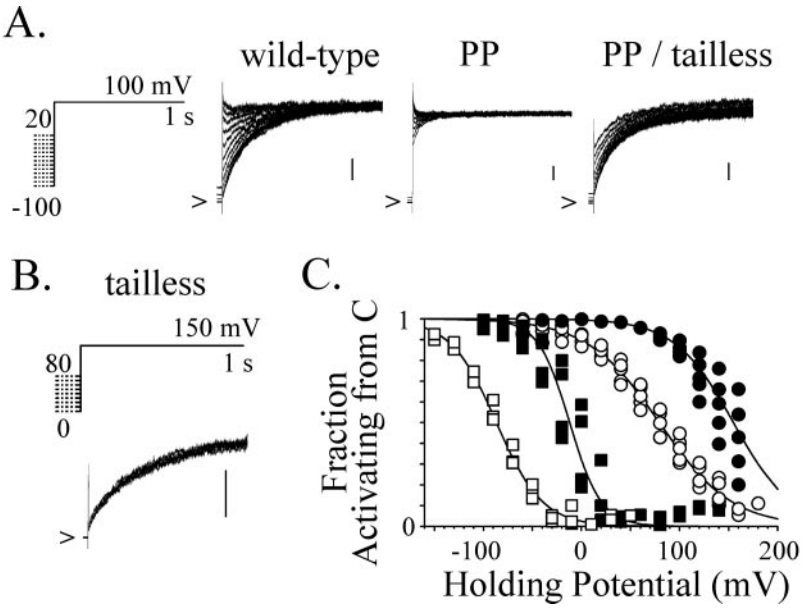

FIGURE 3 Effect of PP and tail deletion mutations on C-state voltage- and K^+-dependence. (*A*) The fraction of channels activating slowly from C as opposed to rapidly from R was assessed as a function of holding potential in wild-type, PP mutant (T322I), and a tailless PP double mutant (T322I, Q546*). For the wild-type channel activation from a −100 mV holding potential is exclusively from C, whereas activation from more positive holds is increasingly from R. PP mutation largely abolishes and additional tail deletion more than restores C distribution. (*B*) Activations of the tailless (Q546*) mutant in the absence of the PP mutation. A more positive voltage range was used and higher amounts of RNA were injected than in *A* because the tailless channel remains largely in C even at +100 mV. (*C*) The fraction of currents activating from C as a function of holding potential and external K^+ concentration for the wild-type and tailless (Q546*) channels. Symbol shape indicates allele (*square* = wild-type, *circle* = Q546*) and color indicates external K^+ concentration (*white* = 1.4 mM K^+, *black* = 140 mM K^+). All recordings are from excised macropatches from TOK1-expressing oocytes. Bath solutions contained 140 mM KCl, 4 mM $MgCl_2$, 1 mM $CaCl_2$, 5 mM EGTA, and 5 mM HEPES, pH 7.5. Pipette solutions were similar but lacked EGTA, contained only 1 mM $MgCl_2$, and in the stated traces in *C* 1.4 mM KCl and 139 mM *N*-methyl D-glucamine (NMG) chloride instead of 140 mM KCl. Calibration bars represent 1 nA and carats indicate 0 current levels.

3 *C*). Tail deletion results in a dramatic positive shift of the C/*V* curve with the tailless V_{50} being 155 ± 22 mV ($n = 5$). Tail deletion causes a roughly parallel shift in the C distribution/voltage (C/*V*) relationship, with the wild-type channel having a 10-fold change in C/R distribution per ~50 mV change and the tailless channel in ~60 mV.

Tail deletion does not substantially alter the $[K^+]_{ext}$-dependence of C distribution. Lowering $[K^+]_{ext}$ from 140 to 1.4 mM results in an approximately 80 mV negative shift in the V_{50} of C distribution for both wild-type and tailless channels (Fig. 3 *C*). In summary, tail deletion does not significantly affect the ability of Tok1 to sense voltage and $[K^+]_{ext}$, instead causing a large parallel shift in both.

Tail deletion alters C/O transition rates

Transition to and from C is complex, generally requiring several rates to describe adequately (Tables 1 and 2). Wild-type C-activation rates are moderately dependent on test potential (Fig. 4 *A*). This increase in the conglomerate rate primarily results from an increase in the rate of the most rapid component (Table 1). At more negative tests, the most rapid rate is in fact not required to describe activation. Activation of the tailless channel can be adequately described with the intermediate and slow components for the wild-type activation (Table 1). Additionally, tailless activation shows no voltage dependence (Fig. 4 *B*, Table 1). Both wild-type and tailless channel activation rates showed only moderate dependence on $[K^+]_{ext}$, conglomerately activating to +100 mV at 4.5 ± 0.4 s^{-1} and 4.7 ± 1.3 s^{-1} in 1.4 mM $[K^+]_{ext}$, respectively.

Tail deletion causes a substantial increase in the apparent rate of deactivation to C. Deactivation rates of the tailless channels to C are >10-fold faster than those of wild-type channels at identical test voltages (Fig. 4, *C* and *D*). Conglomerate deactivation rates are voltage-dependent in both cases, but these dependencies primarily result from change in the distributions rather than a change in the individual deactivation rates (Table 2). In the case of the tailless channel, where deactivation can uniquely be measured at positive potentials, only the single slower rate is required to adequately describe deactivation. Deactivation rates were not dependent on the depolarized conditioning voltage (data not shown). As in the case of activation, both wild-type and tailless deactivation rates displayed little dependence on $[K^+]_{ext}$, conglomerately occurring at ~0.5 and 11 s^{-1} at −100 mV in 1.4 $[K^+]_{ext}$, respectively.

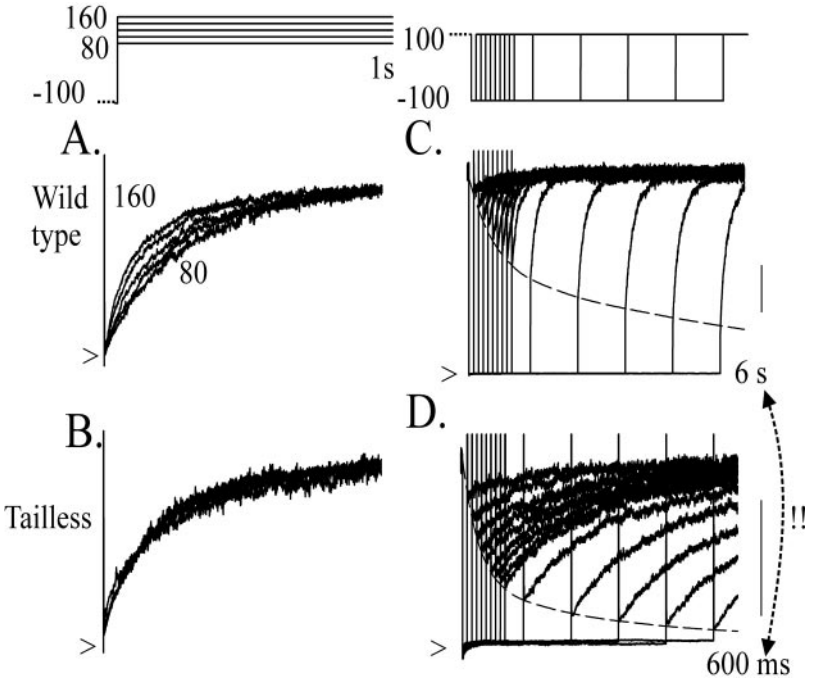

FIGURE 4 C-transition rates of wild-type and tailless channels. Current activations to variable test potentials from wild-type (*A*) and Q546* (*B*) expressing macropatches standardized to maximal current levels. Deactivation rates for wild-type (*C*) and Q546* (*D*) channels were assessed by monitoring resurgence of currents from patches that were conditioned for 10 s to a depolarized activating potential, then deactivated for variable lengths of time at −100 mV. It is important to note that the time scale for the tailless traces in *D* is 10-fold faster than that used for the wild-type channel in *C*. Dotted lines are fits of the peak of the R activations, which thus reflect the time-dependent return of the channel from R to C. Recording conditions were as in Fig. 3 *A*, with ~5-fold more RNA injected for the tailless channel. Calibration bars in *C* and *D* represent 2 nA.

TABLE 1 Activation rates

	Wild-Type				Tailless			
Test (mV)	Conglomerate Rate (s^{-1})	Individual Rates (s^{-1}/Fraction of Total)			Conglomerate Rate (s^{-1})	Individual Rates (s^{-1}/Fraction of Total)		
80	3.0 ± 0.5	fast	—	—	3.2 ± 1.5	fast	—	—
		int.	4.7 ± 2.1	40 ± 17%		int.	6.3 ± 2.4	39 ± 19%
		slow	0.93 ± 0.49	48 ± 17%		slow	0.58 ± 0.22	51 ± 19%
100	3.8 ± 0.6	fast	—	—	3.0 ± 1.2	fast	—	—
		int.	5.5 ± 2.0	48 ± 17%		int.	5.6 ± 1.3	42 ± 15%
		slow	0.92 ± 0.34	41 ± 17%		slow	0.55 ± 0.13	48 ± 15%
120	5.7 ± 0.9	fast	14 ± 8	18 ± 8%	2.9 ± 1.2	fast	—	—
		int.	4.0 ± 1.6	43 ± 19%		int.	5.2 ± 0.9	43 ± 19%
		slow	0.86 ± 0.32	31 ± 15%		slow	0.49 ± 0.11	48 ± 19%
140	8.2 ± 2.2	fast	29 ± 16	22 ± 10%	3.5 ± 1.3	fast	—	—
		int.	4.7 ± 2.2	45 ± 20%		int.	5.3 ± 1.1	46 ± 17%
		slow	0.83 ± 0.38	23 ± 10%		slow	0.63 ± 0.18	49 ± 17%
160	11 ± 2	fast	31 ± 12	23 ± 12%	3.6 ± 1.7	fast	—	—
		int.	7.6 ± 3.4	37 ± 15%		int.	5.3 ± 1.1	46 ± 25%
		slow	1.5 ± 0.6	32 ± 18%		slow	0.53 ± 0.12	43 ± 25%

Activation rates were determined by multiexponential fits of current traces resulting from depolarizations from −100 mV to the stated test potentials. The minimal number of exponents that adequately describe the activations were used. The individual rates are given in terms of magnitude and fraction of the total activating current each component contributes. The conglomerate rate is the summation of the individual rates multiplied by their contributions. All activations in this table were measured in symmetrical 140 mM KCl. All values are given as mean ± SD ($n \geq 3$).

TABLE 2 Deactivation rates

Test (mV)	Wild-Type			Tailless		
	Conglomerate Rate (s^{-1})	Individual Rates (s^{-1}/Fraction of Total)		Conglomerate Rate (s^{-1})	Individual Rates (s^{-1}/Fraction of Total)	
−100	0.87 ± 0.02	1.8 ± 0.1	43 ± 1%	18 ± 5	28 ± 5	58 ± 9%
		0.17 ± 0.08	57 ± 1%		4.6 ± 1.1	42 ± 9%
−50	0.49 ± 0.03	1.4 ± 0.1	30 ± 5%	9.6 ± 3.4	23 ± 4	30 ± 6%
		0.12 ± 0.09	70 ± 5%		4.1 ± 1.2	70 ± 6%
20	—	—	—	4.3 ± 0.2	—	100%
40	—	—	—	4.1 ± 0.3	—	100%
60	—	—	—	3.5 ± 0.3	—	100%
80	—	—	—	3.5 ± 0.5	—	100%

To-C deactivation rates were measured and determined as illustrated in Fig. 4, *C* and *D* upon variable length steps from +100 to the stated deactivation test potential. For the tailless channel, deactivation rates could also be measured directly at positive potentials as time-dependent decay of outward current in response to voltage steps from +100 to the stated potential. Such positive-test deactivations could not be measured with wild-type channels because little change in C-distribution occurs at positive voltages. All values are expressed as in Table 1 and were likewise measured in 140 mM symmetrical KCl.

Tail deletion causes steady-state C dwell at positive potentials

Observed at the single channel level, wild-type TOK1 channels open in bursts lasting generally between 10 and 100 ms, containing submillisecond oscillations (Fig. 5, *A* and *B*). Almost all closures are to an intermediate interburst "IB" state of about equal duration as the open bursts themselves. Neither the closures observed between the bursts (Fig. 6, *A* and *B*) nor the duration of the bursts themselves (Fig. 7, *A* and *B*) shows evidence for voltage dependence. A minor separate peak of longer-lived closures can be discerned probably reflecting rare closures to long-lived C state at these positive potentials.

The single channel behavior of the tailless channel distinctly differs from that of wild-type (Fig. 5, *C* and *D*). Like wild-type, tailless channels dwell in the 10–100 ms duration IB state (Fig. 6, *C* and *D*). Longer closures, though, are much more prevalent in the tailless channel (Fig. 5 *C*). Although the rarity of openings and thus closures at 60 mV thwart a quantitative analysis, qualitatively the duration of these longer-lived closed states appear to be voltage-dependent, lasting on average ~10-fold longer at +60 mV than at +100 mV (Fig. 6, *C* and *D*), consistent with the premise that they reflect closures to C. Also important to note in the single channel behavior of the tailless channel is that multiple transitions between shorter closures, presumably IB, and O often occur between the longer closures to C (Fig. 5 *D*).

Tail deletion decreases open bursting dwell

The expected introduction of C state closures at positive potentials is not the only effect of tail deletion. Although the IB duration remains unaltered, the duration of the bursts themselves is clearly shortened (Fig. 5 *D*). Whereas wild-type channels open in bursts with average durations of ~50

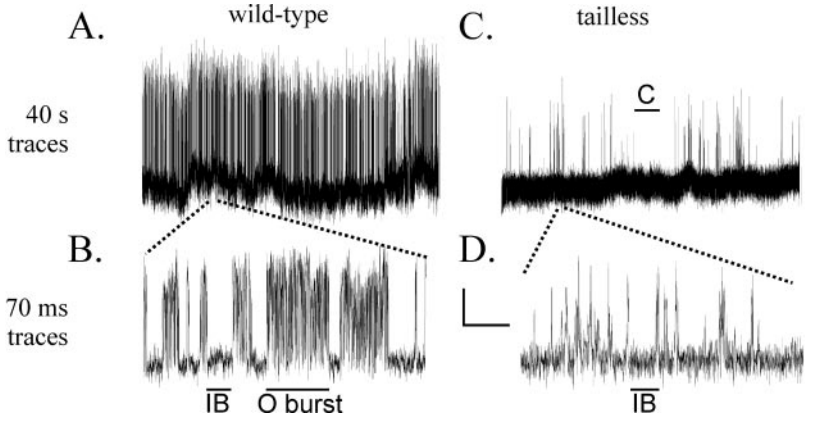

FIGURE 5 Single channel activity of wild-type and mutant channels. Top traces are 40-s traces from single channel patches of wild-type (*A*) and Q546* (*B*) channels at +100 mV in symmetrical 140 mM K^+. Bottom traces (*C* and *D*) are 600-fold expansions of the top traces from the sections of the top traces indicated. Examples of closures typical of C and IB and O bursts are marked. The calibration bar represents 1 pA × 5 s (*top traces*) or 80 ms (*bottom traces*). Bath and pipette solutions were as in Fig. 3 *A*.

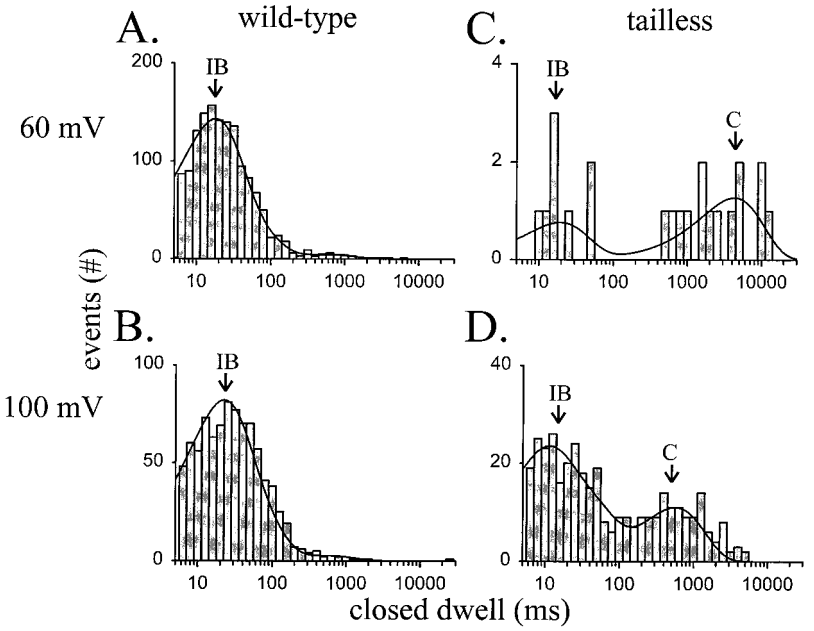

FIGURE 6 Closed-state dwell times. Durations of channel closures were measured from single channel patches for wild-type (*A* and *B*) and Q546* (*C* and *D*) channels at 60 (*A* and *C*) and 100 (*B* and *D*) mV. Closure events are binned on logarithmic time scales. Whereas both wild-type and tailless channels dwell in voltage-independent closed states lasting a few tens of milliseconds on average, the tailless channels readily enter and in fact spend most of there time in voltage-dependent, long-closed C states. Bath and pipette solutions were as in Fig. 3 *A*.

ms (Fig. 7, *A* and *B*), tailless channels open in bursts lasting ~7 ms (Fig. 7, *C* and *D*). Tailless channels, in fact, often open in bursts lasting <1 ms, distinctly raising the possibility that shorter openings may be squelched by acquisition filtration (2 kHz) and thus underestimating the extent of burst-duration shortening caused by tail deletion. In sum-

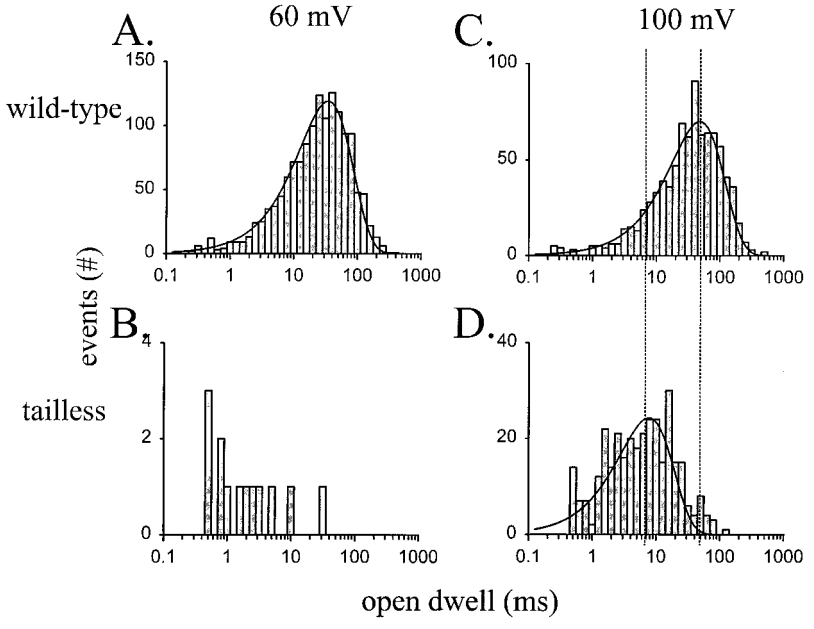

FIGURE 7 Open burst durations. Open channel burst durations of wild-type (*A* and *C*) and Q546* tailless (*B* and *D*) channels are shown. Open burst duration was assessed as the dwell time between closures longer than 5 ms. This burst delimiter was found to accurately distinguish intraburst from interburst closures for both wild-type and tailless channels. Average burst duration of wild-type channels was 50 ms at both 60 and 100 mV and 7 ms for tailless channels at +100 mV. Too few opening events were detectable with the tailless channel at 60 mV to assess the average open time. The same recordings used in Fig. 4 were used for this analysis.

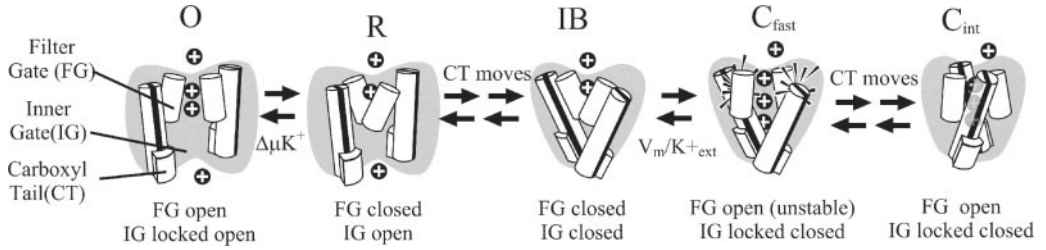

FIGURE 8 Simplified working model of TOK1 gating. In our preferred model, the observed phenomenological states are determined by the positions of the inner gate (IG) and the filter gate (FG) as shown. FG position not only directly determines R and O, but also indirectly IB and C by blocking transition of IG between its open and fast conformation. $C_{fast,}$ C_{int}, and C_{slow} (not shown) are presumed to differ in their closed IG conformations. The carboxyl tail dynamically blocks two IG closures, its open → fast as well as its fast → int transitions. K^+ occupancy of the filter's inner binding site holds FG open, both preventing O to R transition and locking the channel in C. This makes the O/R distribution dependent on the total $\Delta\mu_{K^+}$ because IG is open, whereas the C/IB distribution is dependent only on V_m and $[K^+]_{ext}$. Also critical to the model is the proposal that the "fast" closed conformation of IG interacts unfavorably with the open conformation of FG, as shown for C_{fast}. This simplified cartoon omits many possible manifestations of IG, FG, and CT, which are included in the more comprehensive and detailed diagram presented in Fig. 9 *A*.

mary, tail deletion has two distinct effects apparent at the single channel level: introducing obvious dwell in C at positive potentials and decreasing the duration of the open bursting state.

DISCUSSION

TOK1 is capable of dwelling in several phenomenologically distinct impermeable states: a rapidly transiting, $\Delta\mu_{K^+}$-dependent rectifying "R" state, a voltage-independent interburst "IB" state, and a series of at least three kinetically distinct voltage- and external K^+ ($[K^+]_{ext}$)-dependent closed "C" states, C_{fast}, C_{int}, and C_{slow}. Tail deletion increases the deactivation rate to the C states by ~10-fold (Fig. 4) and inhibits dwell in the C_{fast} state (Table 1) resulting in a >100 mV positive shift in the apparent voltage dependence of C dwell (Fig. 3). In addition to this, tail deletion also increases the deactivation rate from the open bursting state to IB (Figs. 5 and 7). The increase in the IB transition rate and C distribution must result from at least two separate effects of the tail, as will be surmised below. Before speculating how the tail could affect gating, a working model of the gating process itself must first be constructed.

Overview of preferred model of TOK1 gating

Because TOK1's gating is complex, a step-by-step development and refutation of feasible models of the complex gating would be confusing without an overview. We thus first present what we ultimately consider to be the most economical model of gating in a simplified form (Fig. 8). It is based on three parallel interdependent gating mechanisms: an intrinsic filter gating (FG) mechanism, a inner cytoplasmic gate (IG), and the carboxyl tail (CT), which dynamically blocks closure of the IG. Because these are parallel mechanisms, their permutation leads to a multitude of possible states (Fig. 9 *A*), but for now the reader is asked to focus primarily on the simplified cartoon of Fig. 8 for clarity's sake.

As depicted in Fig. 8, the phenomenologically defined open "O," rectifying "R," interburst "IB," and the closed "C" states result from the positions of FG and IG. O results from both FG and IG being open, R being FG closed/IG open, IB being FG closed/IG closed, and the C states being IG closed and FG *open*. The fast, int, and slow C states result from multiple closed conformations IG: IG_{fast}, IG_{int}, and IG_{slow}. Using such a gating scheme, the observed behaviors of the phenomenological states ensue from four basic tenets:

1. The open FG blocks transition of IG;
2. K^+ occupancy of the inner filter-binding site locks FG open;
3. The CT dynamically blocks IG closures, both its open-to-fast and fast-to-int transitions;
4. The open FG interacts unfavorably with the fast-closed conformation of IG, mutually destabilizing each other.

The remainder of the discussion will explain how these simple rules can account for the complex observed behaviors and why alternative models are disfavored.

Interacting gates: voltage/K^+ dependencies of both the R and C states can be accounted for by a single mechanism

The distribution into R and C is dependent on voltage and external K^+, as well as internal K^+ in the case of R. We previously proposed a model of R-state gating in which this dependence results from a collapse of the filter's inner K^+ binding site (Loukin and Saimi, 1999), analogous to the mechanism that is thought to underlie C-type inactivation of *Shaker*-type channels (Kiss and Korn, 1998; Liu et al., 1996; Yang et al., 1997). It was inferred that this collapse is prevented by K^+ occupancy at the filter's inner binding site, while reopening of the collapsed FG required an induced-fit

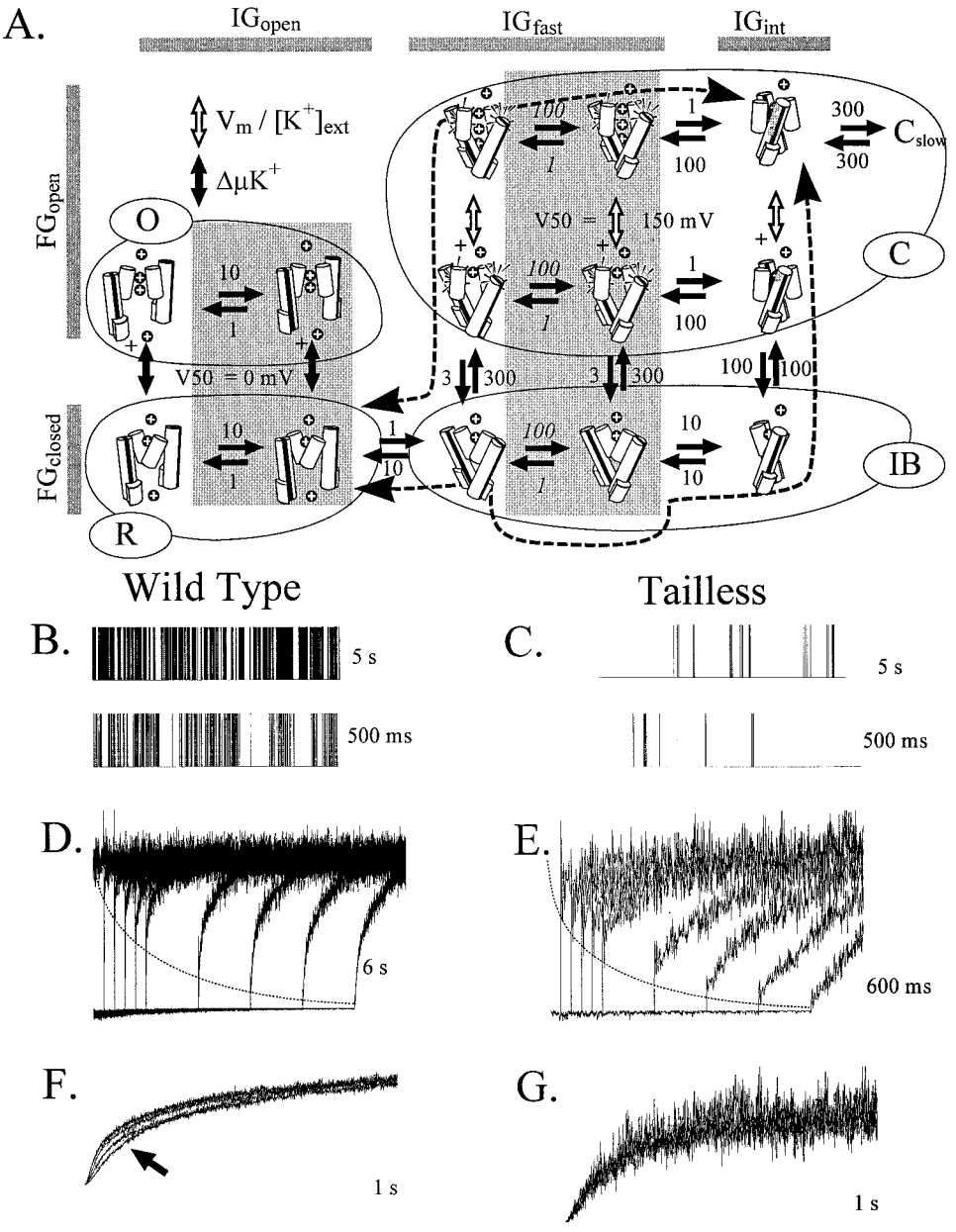

FIGURE 9 Simulation of TOK1 gating. (*A*) A more detailed and comprehensive model of TOK1 gating, based on the simplified model outlined in Fig. 8, which was used for computer simulations. Rows in the array reflect position of the FG, and columns the position of IG, as shown. Corresponding phenomenological states are as shown. Numbers represent approximations of average transition times in milliseconds. Double-ended short arrows represent the voltage-dependent occupancy of the inner filter by K^+, with the stated V_{50} values being the voltage at which half-maximal effective K^+ binding occurs in 100 mM K^+. Transitions within the gray boxes are those that involve movement of the CT and are therefore bypassed by the tailless channel. The two long dotted arrows represent the primary paths the channels take during the simulation of activation and deactivation for the wild-type channel (*upper left path*) and the tailless channel (*lower right path*). (*B*) Representative simulated single channel traces of the wild-type channel lasting 5 s (*top*) or 500 ms (*bottom*) at 100 mV. (*C*) Same as *B* but simulated for the tailless channel. (*D*) Summated deactivation of 10^5 wild-type channels under conditions simulating those used for Fig. 4 *C*. (*E*) Deactivation of the 10^7 tailless channel as in Fig. 4 *D*. (*F*) Activation of 10^5 wild-type channels as in Fig. 4 *A*. Arrow points out voltage-dependence of fast activation rates. (*G*) Activation of 10^7 tailless channels as in Fig. 4 *B*. A description of the simulation's algorithms appears in the Methods section.

reoccupancy of this site by K^+ from the cytoplasm. Residence of the outer site by a K^+ ion either inhibits reoccupancy of the inner site and/or promotes evacuation of the inner site. R/O distribution thus depends on the entire transmembrane $\Delta\mu_{K^+}$, with an inward $\Delta\mu_{K^+}$ forcing FG closure and an outer $\Delta\mu_{K^+}$ promoting its reopening.

To explain $[K^+]_{ext}$ dependency of C, it would be most economical to propose that the K^+/voltage-dependent dis-

tribution into C relies on the same mechanism, i.e., the ability of K^+ occupancy to lock FG open. Such dependence could result if the open FG locked the IG (tenet 1), for instance by sterically preventing the movement of the IG helix between its open (IG_{open}) and closed form (Fig. 8). The ability of internal K^+ to affect R but not C distribution would naturally result from the occlusion of the inner pore by IG. A potential point of confusion is that inward $\Delta\mu_{K^+}$ is proposed to lock FG open in the case of C, yet favor FG closure in the case of R. In the case of R, inward $\Delta\mu_{K^+}$ could drive K^+ out of the filter's inner site into the cytoplasm, allowing collapse of FG (tenet 2). When IG is closed, though, an equilibrium condition exists because K^+ cannot exit internally and an inward $\Delta\mu_{K^+}$ will saturate the filter, jamming FG open, and hence locking IG closed (tenet 1; Fig. 8, C states).

It should be noted that other, more complex scenarios are viable to account for C's voltage-dependence. Although TOK1 has no recognizable S4-like voltage sensor, it has charged residues elsewhere that could act as voltage sensors (i.e., K^+ does not *necessarily* have to be the gating charge as proposed). Such a mechanism is complicated, though, by the need to evoke a parallel K^+-sensing mechanism. Even if binding of K^+ within the membrane's field is indeed the mechanism, this binding does not *necessarily* need to occur in the pore. Given the steepness of the C/*V* relationship, though, extra-pore binding sites would have to be buried significantly within the membranes field, requiring the evocation of a sizable crevasse parallel to the pore. Our preferred FG-centered model based on tenets 1 and 2 is by far the most economical mechanism because it does not require additional channel structures, and accounts for the voltage-dependence of R and C with a single mechanism.

The carboxyl tail alters at least two transitions

Given this preferred model of gating, how might the tail interact with such gating machineries to account for its dramatic effects when deleted? Before considering this, a fundamental issue must be addressed: does deleting the tail remove a specific natural function or merely induce a pathological overall rearrangement of protein structure? Evidence suggests the former. First, other important channel parameters, such as unitary conductance, ionic selectivity, degree of K^+-dependence, and the activation kinetics from the two more stable C states remain unchanged in the tailless channel, arguing against overall structural rearrangement. Second, although the deletion of the terminal 250 amino acids is indeed a gross alteration, T322I alone can restore near wild-type behavior to the PP-tailless double mutant (Fig. 3). This argues against global structural rearrangement being the underlying cause of the tail deletion effect.

Alteration of only a single transition cannot explain *both* the decreased O burst duration and the increased propensity toward C. An O ↔ IB ↔ C serial arrangement has been implicitly assumed in the modeling so far. The only way that an increase in the transition rate to C could cause a decrease in burst duration was if IB was not an obligatory intermediate between O and C, e.g., IB ↔ O ↔ C, with premature burst termination resulting not from an increased deactivation rate to IB, but from a dramatically increased rate to C. Although the transition time to C is decreased ~10-fold by tail deletion, from ~1 to ~0.1 s (Fig. 4, *C* and *D*), this is still nowhere near ~1 ms, i.e., the tailless burst duration. Furthermore, the short IB closures of the tailless channels show little voltage-dependence (Fig. 6; although the lack of datapoints at 60 mV weakens this argument). The most direct explanation of decreased burst duration is that tail deletion simply increases the O to IB transition rate.

Conversely, an increase in the O to IB rate alone cannot account for the large positive shift in the C/*V* relationship (Fig. 3). The wild-type O ↔ IB transition rates are nearly symmetrical, as evidenced by the roughly similar length of IB closures and O bursts (Figs. 5 *B*, 6, and 7). Assuming a serial O ↔ IB ↔ C relationship where the IB ↔ C transition is voltage-dependent, even an infinite increase in the O to IB rate would thus only cause a maximum twofold increase in the "substrate" for the voltage-dependent transition, IB (i.e., wild-type channels would be approximately half in O, half in IB, whereas tailless channels would be near-exclusively in IB). Assuming a voltage-dependent Boltzmann distribution between C and IB:

$$\mathrm{IB/C} = \exp(-zF(V - V_{50})/RT)$$

Then the twofold increase in the IB concentration of the tailless channel compared to that of wild type would result in only a $RT \ln 2/zF$, or ~20 mV change in the apparent V_{50} given the steepness of the C/*V* relationship (Fig. 3 *C*). This is nowhere near the observed >100 mV change.

In summary, the decreased burst duration cannot be accounted for by the observed changes in the deactivation rate to C, nor can the change in the C distribution be accounted for by an increased O → IB rate alone. Thus, tail deletion must alter at least two separate gating transitions, one between O and IB, and another somewhere else in the deactivation to C.

"Foot in the door": evidence that CT dynamically prevents IG closures

It is easier to consider the tail's effect on O → IB first, although it is not the cause of the primary effect of tail deletion: the large shift in the C/*V* relationship. This is because the deletion-induced increase in this rate cannot be accounted for by a change in voltage-sensing/K^+ binding, because this transition is voltage-independent (Fig. 7). It is therefore likely that the tail acts directly on the gating process itself here.

Two classes of mechanisms could be envisioned: dynamic and static. In static mechanisms, the simple presence of the tail would simply stabilize the O state relative to IB. In dynamic mechanisms, the tail must move before IG closure could occur. The simplest manifestation of a dynamic mechanism would be a "foot-in-the-door" scenario in which the tail interacted with IG in such a way as to block its closure (Fig. 8, R to IB transition).

The unidirectional effect of tail deletion, increasing the O to IB (shorter burst duration, Fig. 7) but not the IB to O rate (similar IB duration, Fig. 6), favors the foot-in-the-door mechanism. In this scenario, the tailed channel must pass through an O′ state (Fig. 8, left "CT moves" step, left shaded portion of Fig. 9 *A*), which differed from O in that the foot (tail) was out of the way of the door (IG), on its way to IB. Tail deletion would eliminate this step and thus speed $O \rightarrow IB$, but not the $O \leftarrow IB$ transition.

As to the role of the tail in C-state gating, the most economical scheme is to extend the "foot-in-the-door" model. The tail would interact with IG in three different conformations: the one proposed above, which blocks the initial open → fast closing (Fig. 8, R to IB transition); an additional one, which permits fast closing but blocks further fast → intermediate IG closing (Fig. 8, $C_{fast} \rightarrow C_{int}$ transition); and one that allowed IG to close fully. To cause the >100 mV shift in the C/*V* relationship there must be at least a 100/1 bias for the tail to reside in the IG_{int}-blocking conformation when in the IG_{fast} conformation, as proposed in Fig. 9 *A* (*right shaded box*). Having the tail block the $C_{fast} \rightarrow C_{int}$ transition can readily explain many of the observed C-state behaviors of the tailless TOK1, including the large shift in the C/*V* relationship and the loss of the C_{fast} component of activation. Because of the complexity of the model, Monte Carlo computer simulations were performed to verify this claim.

Model predicts many aspects of TOK1 gating

Fig. 9 *A* details TOK1 gating used to test our model for Monte Carlo computer simulation. The intention is not to derive parameters, but to show that much of the observed wild-type and tailless behavior can be qualitatively predicted by the model. Semi-order-of-magnitude estimates of time constants (in milliseconds) or rough estimates of apparent V_{50} values of voltage dependence in 100 mM symmetrical K^+ were assigned to each transition and used to determine probabilities of state transitions assigned by random rolls (see Methods). The estimated V_{50} of K^+ binding that locks the channel in C, 150 mV, is substantially positive to the observed V_{50} of C dwell of the wild-type but not the tailless channel (Fig. 3 *C*). This is because the bias caused by CT blocking of the $IG_{fast} \rightarrow IG_{int}$ transition, proposed to be 100/1 in the model (Italicized transitions in Fig. 9), favors partitioning toward O. The V_{50} of C partitioning of the tailless is near that of C-locking K^+ binding because it lacks this biased transition, and the remaining transitions are not O-favoring in net. Due to tenet 4, that the open FG interacts unfavorably with the fast conformation of IG, there exists a strong bias of the $IG_{fast} \rightarrow IG_{int}$ transition when FG is open (i.e., $C_{fast} \rightarrow C_{int}$). Whereas the wild-type channel overcomes this bias by the compensatory IG_{fast}-favoring bias of CT interaction, the tailless channel cannot, which accounts for the loss of C_{fast} dwell in the mutant (Table 1).

The single channel behaviors of both types of channels (Fig. 5) are similar to those predicted by the simulation (Fig. 9, *B* and *C*). This includes the interburst behavior of wild-type and tailless channels and the preponderance of C-state closures in the tailless channel at positive voltages. Note that the flickery behavior of the channels does not result from an attempt at a realistic simulation of the R state, because that is a nonequilibrium process that could not be simulated with the algorithms used (see Methods).

The simulations predicted the rapid component of the to-C deactivation rates upon depolarization (Fig. 9, *D* and *E*; note: the slower component of deactivation is not accounted for in our model). Reviewing the state transitions during the simulation revealed that the tailless channels primarily deactivate through the lower right pathway of Fig. 9 (*lower right broken arrow*), while the wild-type channels primarily deactivated through the upper left pathway (*upper right broken arrow*), being excluded from the more rapidly deactivating path by the bias of the CT movement preceding the transition from IG_{fast} (FG_{closed}) → IG_{slow} (FG_{closed}).

Activation rates are also closely simulated (Fig. 9, *F* and *G*), including the voltage-dependence of C_{fast} exclusively in the wild-type channel (Fig. 9 *F*, *arrow*). Qualitatively, this voltage-dependence results from the bias toward O in the tailed but not the tailless channel. Consequently, there is a strong voltage-dependence in the ratio of the initial K^+-evacuated C state following depolarization (i.e., initial substrate) to the ultimate steady-state O concentration (i.e., final substrate) at moderately positive potentials. Although not a proof of the validity of our model or a disproof of others, the ability of the simulations to describe these behaviors simply attests to its viability.

Possible physiological functions of such regulation of TOK1 activity remain a mystery. Since regulatory modification has been demonstrated in other cytoplasmic tails involved in channel gating (Maingret et al., 1999, 2000; Murakoshi et al., 1997; Patel et al., 1999; Schreiber et al., 1999; Varnum and Zagotta, 1997), it is tempting to conclude that modification of the tail by cytoplasmic signaling systems could essentially modulate TOK1 between a tailed and at least partially tailless form. Consistent with this idea is the recent finding by Sesti et al. (2001) that cytoplasmic exposure to yeast K1 killer toxin specifically lengthens the duration of TOK1's long closed states. It may be that K1 binds to the tail, inhibiting its function, and thereby promoting dwell in the longer-lived C states.

We thank C. Kung and C. Palmer for critical reading of the manuscript.

This work was partially supported by National Institutes of Health Grant GM 54867.

REFERENCES

Bach, M. L., F. Lacroute, and D. Botstein. 1979. Evidence for transcriptional regulation of orotidine-5′-phosphate decarboxylase in yeast by hybridization of mRNA to the yeast structural gene cloned in *Escherichia coli*. *Proc. Natl. Acad. Sci. U.S.A.* 76:386–390.

Cushman, S. J., M. H. Nanao, A. W. Jahng, D. DeRubeis, S. Choe, and P. J. Pfaffinger. 2000. Voltage dependent activation of potassium channels is coupled to T1 domain structure. *Nat. Struct. Biol.* 7:403–407.

Czempinski, K., T. E. Zimmermann, and B. Müller-Röber. 1997. New structure and function in plant K^+ channels: KCO1, an outward rectifier with a steep Ca^{2+} dependency. *EMBO J.* 16:2565–2575.

Derst, C., and A. Karschin. 1998. Evolutionary link between prokaryotic and eukaryotic K+ channels. *J. Exp. Biol.* 201(Pt 20):2791–2799.

Duprat, F., F. Lesage, M. Fink, R. Reyes, C. Heurteaux, and M. Lazdunski. 1997. TASK, a human background K^+ channel to sense external pH variations near physiological pH. *EMBO J.* 17:5464–5471.

Gordon, S. E., and W. N. Zagotta. 1995a. A histidine residue associated with the gate of the cyclic nucleotide-activated channels in rod photoreceptors. *Neuron.* 14(1):177–183.

Gordon, S. E., and W. N. Zagotta. 1995b. Localization of regions affecting an allosteric transition in cyclic nucleotide-activated channels. *Neuron.* 14:857–864.

Gustin, M. C., B. Martinac, Y. Saimi, M. R. Culbertson, and C. Kung. 1986. Ion channels in yeast. *Science.* 233:1195–1197.

Ketchum, K. A., W. J. Joiner, A. J. Sellers, L. K. Kaczmarek, and S. A. Goldstein. 1995. A new family of outwardly rectifying potassium channel proteins with two pore domains in tandem. *Nature.* 376:690–695.

Kiss, L., and S. J. Korn. 1998. Modulation of C-type inactivation by K^+ at the potassium channel selectivity filter. *Biophys. J.* 74:1840–1849.

Lesage, F., E. Guillemare, M. Fink, F. Duprat, M. Lazdunski, G. Romey, and J. Barhanin. 1996. A pH-sensitive yeast outward rectifier K^+ channel with two pore domains and novel gating properties. *J. Biol. Chem.* 271:4183–4187.

Liu, Y. M., M. E. Holmgren, M. E. Jurman, and G. Yellen. 1997. Gated access to the pore of a voltage-dependent K^+ channel. *Neuron.* 19: 175–184.

Liu, Y., M. E. Jurman, and G. Yellen. 1996. Dynamic rearrangement of the outer mouth of a K^+ channel during gating. *Neuron.* 16:859–867.

Loukin, S. H., and Y. Saimi. 1999. K^+-dependent composite gating of the yeast K^+ channel, Tok1. *Biophys. J.* 77:3060–3070.

Loukin, S. H., B. Vaillant, X-L. Zhou, E. P. Spalding, C. Kung, and Y. Saimi. 1997. Random mutagenesis reveals a region important for gating of the yeast K^+ channel, Ykc1. *EMBO J.* 16:4817–4825.

Maingret, F., I. Lauritzen, A. J. Patel, C. Heurteaux, R. Reyes, F. Lesage, M. Lazdunski, and E. Honore. 2000. TREK-1 is a heat-activated background K^+ channel. *EMBO J.* 19:2483–2491.

Maingret, F., A. J. Patel, F. Lesage, M. Lazdunski, and E. Honore. 1999. Mechano- or acid stimulation, two interactive modes of activation of the TREK-1 potassium channel. *J. Biol. Chem.* 274:26691–26696.

Minor, D. L., Y. F. Lin, B. C. Mobley, A. Avelar, Y. N. Jan, L. Y. Jan, and J. M. Berger. 2000. The polar T1 interface is linked to conformational changes that open the voltage-gated potassium channel. *Cell.* 102: 657–670.

Murakoshi, H., G. Shi, R. H. Scannevin, and J. S. Trimmer. 1997. Phosphorylation of the Kv2.1 K^+ channel alters voltage-dependent activation. *Mol. Pharmacol.* 52:821–828.

Patel, A. J., E. Honore, F. Lesage, M. Fink, G. Romey, and M. Lazdunski. 1999. Inhalational anesthetics activate two-pore-domain background K^+ channels. *Nat. Neurosci.* 2:422–426.

Reid, J. D., W. Lukas, R. Shafaatian, A. Bertl, C. Scheurmann-Kettner, H. R. Guy, and R. A. North. 1996. The *S. cerevisiae* outwardly rectifying potassium channel (*DUK1*) identifies a new family of channels with duplicated pore domains. *Receptors and Channels.* 4:51–62.

Schreiber, M., A. Yuan, and L. Salkoff. 1999. Transplantable sites confer calcium sensitivity to BK channels. *Nat. Neurosci.* 2:416–421.

Sesti, F., T. M. Shih, N. Nikolaeva, and S. A. Goldstein. 2001. Immunity to K1 killer toxin: internal TOK1 blockade. *Cell.* 105:637–644.

Shimbo, K., D. L. Brassard, R. A. Lamb, and L. H. Pinto. 1995. Viral and cellular small integral membrane proteins can modify ion channels endogenous to *Xenopus* oocytes. *Biophys. J.* 69:1819–1829.

Tzounopoulos, T., J. Maylie, and J. P. Adelman. 1995. Induction of endogenous channels by high levels of heterologous membrane proteins in *Xenopus* oocytes. *Biophys. J.* 69:904–908.

Varnum, M. D., and W. N. Zagotta. 1997. Interdomain interactions underlying activation of cyclic nucleotide-gated channels. *Science.* 278: 110–113.

Vergani, P., T. Miosga, S. M. Jarvis, and M. R. Blatt. 1997. Extracellular K^+ and Ba^{2+} mediate voltage-dependent inactivation of the outward-rectifying K^+ channel encoded by the yeast gene *TOK1*. *FEBS Lett.* 405:337–344.

Yang, Y., Y. Yan, and F. J. Sigworth. 1997. How does the W434F mutation block current in *Shaker* potassium channels? *J. Gen. Physiol.* 109: 779–789.

Zhou, X. L., B. Vaillant, S. H. Loukin, C. Kung, and Y. Saimi. 1995. *YKC1* encodes the depolarization-activated K^+ channel in the plasma membrane of yeast. *FEBS Lett.* 373:170–176.

Zilberberg, N., N. Ilan, R. Gonzalez-Colaso, and S. A. N. Goldstein. 2000. Opening and closing of KCNKO potassium leak channels is tightly regulated. *J. Gen. Physiol.* 116:721–734.